Journal of Power Sources 191 (2009) 473–482

Contents lists available at ScienceDirect

Journal of Power Sources

journal homepage: www.elsevier.com/locate/jpowsour

Multiple model predictive control for a hybrid proton exchange membrane fuel cell system

Qihong Chen[a,*], Lijun Gao[b], Roger A. Dougal[b], Shuhai Quan[a]

[a] School of Automation, Wuhan University of Technology, 205 Luoshi Rd, Hongshan District, Wuhan 430070, China
[b] Department of Electrical Engineering, University of South Carolina, Columbia, SC 29208, USA

ARTICLE INFO

Article history:
Received 19 December 2008
Received in revised form 11 February 2009
Accepted 11 February 2009
Available online 24 February 2009

Keywords:
PEM fuel cell
Hybrid vehicle
Predictive control
Power management
Oxygen control
Ultracapacitor

ABSTRACT

This paper presents a hierarchical predictive control strategy to optimize both power utilization and oxygen control simultaneously for a hybrid proton exchange membrane fuel cell/ultracapacitor system. The control employs fuzzy clustering-based modeling, constrained model predictive control, and adaptive switching among multiple models. The strategy has three major advantages. First, by employing multiple piecewise linear models of the nonlinear system, we are able to use linear models in the model predictive control, which significantly simplifies implementation and can handle multiple constraints. Second, the control algorithm is able to perform global optimization for both the power allocation and oxygen control. As a result, we can achieve the optimization from the entire system viewpoint, and a good tradeoff between transient performance of the fuel cell and the ultracapacitor can be obtained. Third, models of the hybrid system are identified using real-world data from the hybrid fuel cell system, and models are updated online. Therefore, the modeling mismatch is minimized and high control accuracy is achieved. Study results demonstrate that the control strategy is able to appropriately split power between fuel cell and ultracapacitor, avoid oxygen starvation, and so enhance the transient performance and extend the operating life of the hybrid system.

1. Introduction

Proton exchange membrane (PEM) fuel cells are clean and highly efficient electrochemical devices that convert hydrogen directly into electricity. They have been considered as alternative power sources for vehicles, mobile robots, backup power sources, etc. In practical applications, PEM fuel cells are usually arranged with auxiliary power sources, such as batteries and ultracapacitors, to form hybrid systems.

The electric loads supplied by a hybrid fuel cell system may frequently fluctuate. Abrupt changes in power may cause oxygen starvation in the fuel cell, may overcharge or overdischarge the ultracapacitor, and may reduce the working life of the system in a long term [1,2]. Therefore, sophisticated power management and oxygen control are necessary.

Many studies have been carried out on power management. Jiang et al. [3] present an adaptive control strategy that adjusts the output current set point of the fuel cell. Ferreira et al. [4] studied a fuzzy logic supervisory-based power management strategy for a fuel cell/ultracapacitor/battery combined electric vehicle. Guezennec et al. [5] and Rodatz et al. [6] designed an optimal control strategy to minimize the hydrogen consumption in a hybrid fuel cell system. Zhang et al. [7] proposed a wavelet-transform algorithm to identify and allocate power demands with different frequency contents to corresponding sources to achieve an optimal power management control algorithm.

In the aspect of oxygen control, Pukrushpan et al. [8,9] developed a mechanistic model suitable for the study of controls in fuel cell systems. Vahidi et al. [1,10] used a theoretical model-based predictive control approach to manage current and oxygen so as to avoid oxygen starvation and surge or choking of the air compressor in a fuel cell/ultracapacitor hybrid system. To enforce constraints on the oxygen supply and protect the fuel cells from oxygen starvation, Sun and Kolmanovsky [11] use a robust load governor to regulate the current drawn from the fuel cell. These strategies have all proved effective in avoiding oxygen starvation.

Model predictive control (MPC) works in a centralized manner for constrained control problems through a multivariable minimization [12]. A key advantage of MPC over other control schemes is the ability to deal with constraints in a systematic and straightforward manner [13]. Multiple model adaptive control has been widely utilized in improving the transient response of systems with boundary condition changes [14].

We have noticed that power management and oxygen control are typically investigated separately. That is to say, power distribu-

* Corresponding author. Tel.: +86 27 8785 9049; fax: +86 27 8764 0549.
E-mail address: chenqh@whut.edu.cn (Q. Chen).

0378-7753/$ – see front matter © 2009 Elsevier B.V. All rights reserved.
doi:10.1016/j.jpowsour.2009.02.034

tion command is determined first according to load requirement but without interacting with real-time fuel cell control, and then fuel cell system control (in which including oxygen supply control) is determined to respond to the power command signal while not to the load requirement directly. As a result, the hybrid system control is not global optimized. Our purpose in this paper, then, is to describe a centralized multiple models-based predictive control scheme that addresses both power distribution and oxygen control, and that can provide a systematic and globally optimized solution under multiple constraints.

The proposed control scheme is designed and implemented as follows. First, characteristics of the hybrid system over its whole operating range are identified and expressed as multiple linear discrete-time models by employing the fuzzy clustering technology. Each model corresponds to a typical operating zone of the hybrid system, and the models are updated online to cater for parameter variations of the real system. Second, constrained MPCs are designed for each model. Finally, an upper-layer adaptive switch is designed to determine the most appropriate model and to switch the corresponding MPC as needed. The control scheme is aimed to enhance the performance of the system, and to protect the hybrid system not only by avoiding oxygen starvation, but also by trading off transient demands between the fuel cell and the ultracapacitor, according to constraints and weighting matrices of the output errors.

The paper is organized as follows. In Section 2, structure and description of the predictive control using multiple models are introduced. Section 3 describes dynamic modeling of the hybrid system. Controllers are designed in Section 4. In Section 5, we implement and discuss experiment and simulation results. Conclusions are given in Section 6.

2. System structure and description

We focus on control of electric power and of the oxygen supply. We assume that the hydrogen is supplied at constant and appropriate pressure, humidity, and temperature, and that wave effects are insignificant. These assumptions should not undermine the validity of our work because pressure, temperature and humidity dynamics are much slower than the fuel cell power dynamics which we study in this paper [1].

2.1. System description

The hybrid fuel cell system studied in this paper, as shown in Fig. 1, is designed for an automobile application. The electrical outputs of two PEM fuel cell stacks are directly connected in parallel to the propulsion motor load. An ultracapacitor bank is also connected to the load through a bi-directional DC/DC converter to form a hybrid PEM fuel cell/ultracapacitor system. The ultracapacitor bank should supply peak power and should be recharged by the fuel cell. The hybrid system can be quite efficient because the fuel cell directly supplies the bulk of the load demand while the DC/DC converter only operates to meet transient demands.

The distribution of power between the fuel cell and the ultracapacitor depends on the duty ratio of the DC/DC converter, while the oxygen supply to the PEM fuel cell is regulated by the voltage applied to the air compressor, V_{cm}. Duty ratio of a DC/DC converter is defined as the ratio of switch on time interval, T_{ON}, to switching period T, i.e.

$$d = \frac{T_{ON}}{T}. \tag{1}$$

There exist two duty ratios in the bi-directional DC/DC converter. One duty ratio, d_c, is for charging the ultracapacitor, and the other, d_d, is for discharging the ultracapacitor.

Oxygen excess ratio is defined as

$$\lambda_{O_2} = \frac{W_{O_2,in}}{W_{O_2,rct}}, \tag{2}$$

where $W_{O_2,in}$ is the flow of oxygen into the fuel cell and $W_{O_2,rct}$ is the mass of oxygen reacted in the fuel cell and is related to the current drawn from the fuel cell.

The state of charge is usually defined as the ratio of energy stored in the ultracapacitor to the rated energy capacity of the ultracapacitor [15], i.e.

$$\overline{SOC} = \frac{V_c^2}{V_{c,max}^2}, \tag{3}$$

where V_c and $V_{c,max}$ are the instantaneous voltage and maximum voltage of the ultracapacitor, respectively. $V_{c,max}$ is constant and controlling $\overline{SOC}$ is equivalent to controlling $V_c/V_{c,max}$. As a result, we define a new state of charge, SOC, which is easier to control [1], i.e.

$$SOC = \frac{V_c}{V_{c,\max}}. \tag{4}$$

2.2. Control structure and principle

The framework of the multiple model predictive control is presented in Fig. 2. It has four major blocks, namely model predictive controllers, models, adaptive switch, and the controlled system.

There are n linear models and corresponding MPCs in the system. Namely, $Model_i$ ($i = 1, 2, \ldots, n$) is the ith linear model of the hybrid system at a typical operating zone and MPC_i is a model predictive controller designed for $Model_i$. $Model_{online}$ denotes the unit that updates each model online according to real-time data so as to cater for time variation of the system.

The adaptive switch, also called an upper-layer controller, is a decision unit that determines the most appropriate MPC to control the hybrid system during each control period. Briefly, its operating principle is as follows. Firstly, control signals are fed into the hybrid system and into each model simultaneously. Secondly, the output of each model is compared to the actual output, respectively. Finally, according to the errors, the adaptive switch periodically chooses the model that best matches the observed performance and then switches on the corresponding MPC. At each period, only one MPC is in service and occupies computational resources.

The system design consists of two major steps: identification of the hybrid system and design of the control. System identification consists of collecting input and output data from the hybrid system and dividing it into several sets based on fuzzy clustering. Then models are identified from each data set. Control design entails design of the MPCs and design of the adaptive switch. In designing the MPCs, we will focus on handling multiple constraints and enhancing computational speed. In design of the adaptive switch, it is important to design performance evaluation function and the switch mechanism.

3. Modeling of the hybrid system

The hybrid system is a multiple input and multiple output nonlinear system. This section establishes the bank of linear models that describe the hybrid system. Input and output data are divided into multiple sets through fuzzy clustering firstly and then the model for each data set is identified. In addition, the models will be updated online during utilization phase.

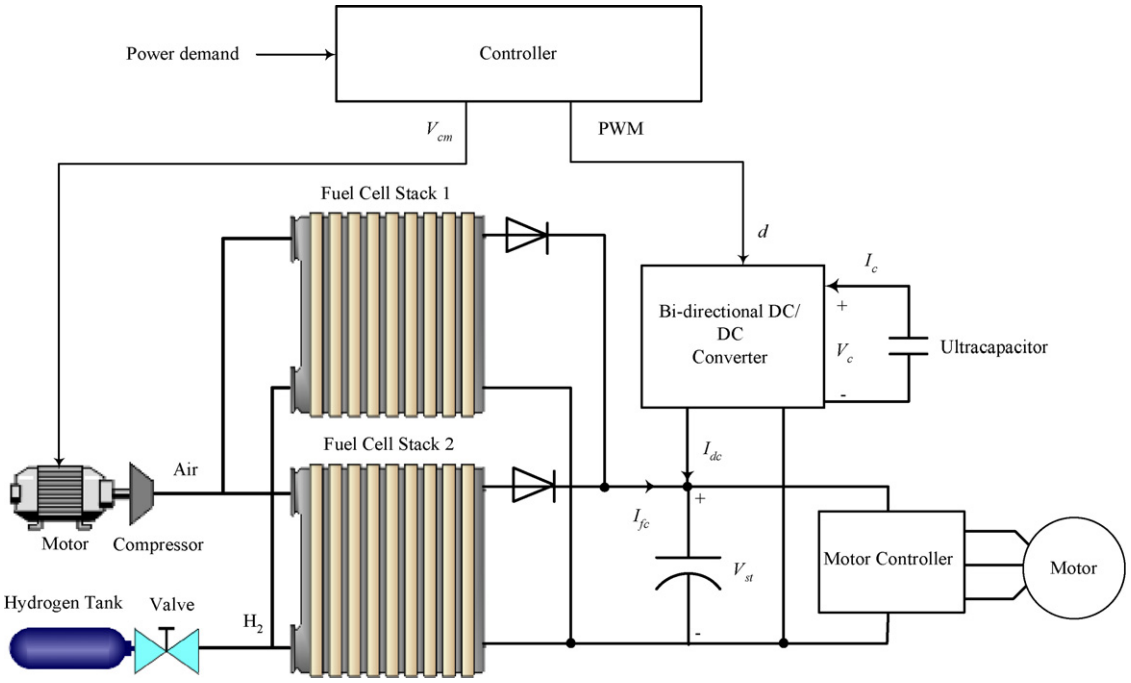

Fig. 1. Schematic of the hybrid PEM fuel cell system.

3.1. Fuzzy clustering

To characterize the hybrid system using piecewise linear models, fuzzy clustering is chosen to divide the input and output data into multiple sets corresponding to linear areas. It contains three steps: determine input and output variables, collect input and output data, and classify data using fuzzy clustering method. The input and output variables are first determined as follows.

Input variables are chosen as

$$u(k) = \begin{pmatrix} V_{cm} & d_d & d_c \end{pmatrix}^T, \tag{5}$$

Output variables are chosen as

$$y(k) = \begin{pmatrix} \lambda_{O_2} & W_{cp} & p_{sm} & V_{st} & I_{st} & I_c & SOC \end{pmatrix}^T, \tag{6}$$

where W_{cp} is air flow of compressor, p_{sm} is pressure of air supply manifold, V_{st} is voltage of the fuel cell, I_{st} is current of the fuel cell, and I_c is current of the ultracapacitor. Power demanded by the load, P_d, is viewed as a disturbance to the system. The hybrid system can now be characterized by these input and output variables.

$$z_i = \begin{pmatrix} y^T(i) & u^T(i) \end{pmatrix}^T, \quad i = 0, 1, 2, \ \ldots, \ N-1, \tag{7}$$

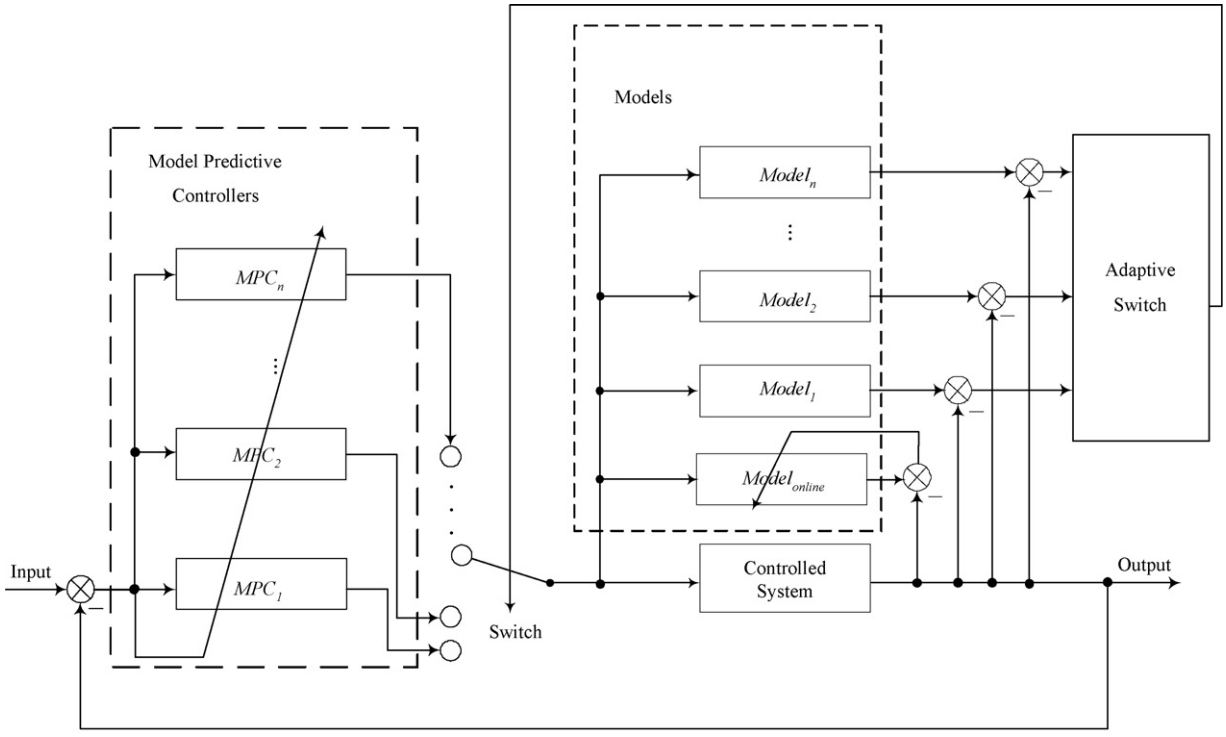

Fig. 2. Framework of multiple model predictive control.

where N denotes the total number of sampled data. $u(i) \in \mathbf{R}^3$, $y(i) \in \mathbf{R}^7$, and $z(i) \in \mathbf{R}^{10}$.

After the input and output data of the system are collected, a fuzzy clustering approach with a fuzzy covariance matrix [16] is applied to classify the data into n sets. The kernel issue of the method is to minimize the cost function

$$J_f = \sum_{i=0}^{N-1}\sum_{j=1}^{n} \omega_{ij}^{\alpha} d_{ij}(\theta_j) + \sum_{i=0}^{N-1} \lambda_i \left(\sum_{j=1}^{n} \omega_{ij} - 1 \right) + \sum_{j=1}^{n} \beta_j (|M_j| - \rho_j), \tag{8}$$

where ω_{ij} is a membership function of sample z_i to the jth class, α is a smoothing parameter, $d_{ij}(\theta_j)$ denotes the distance from point z_i to the center v_j of the jth class and

$$d_{ij}(\theta_j^{(k)}) = (z_i - v_j)^T M_j (z_i - v_j), \tag{9}$$

$M_j \in \mathbf{R}^{10\times 10}$ is a symmetric and positive definite weighting matrix, $\theta_j = (v_j, M_j)$, the superscript k represents the step number of the iterative computing cycle, λ_i and β_i are Lagrange multipliers, ρ_j is a constraint of $|M_j|$.

Given data $\{z_i\}$ and an initial guess $\theta_j^{(0)}$, the classification is proceeded as the following iterative algorithm.

For $k = 1, 2, \ldots$, use the computing results of the $(k-1)$th cycle to compute the variables of the kth cycle:

(i) Compute the distance from point z_i to the jth class according to Eq. (9).

(ii) Compute $\omega_{ij}^{(k)}$

$$\omega_{ij}^{(k)} = \left(\sum_{l=1}^{n} \left(\frac{d_{ij}}{d_{il}} \right)^{1/(\alpha-1)} \right)^{-1}. \tag{10}$$

If $d_{ih} = 0$ for some h, set $\omega_{ih} = 1$, $\omega_{il} = 0\ \forall l \neq h$

(iii) Compute new estimates $v_j^{(k)}$, $M_j^{(k)}$

$$v_j^{(k)} = \frac{\sum_{i=0}^{N-1} \omega_{ij}^{\alpha} z_i}{\sum_{i=0}^{N-1} \omega_{ij}^{\alpha}}, \tag{11}$$

$$M_j^{(k)} = \left\{ \left(\frac{1}{\rho_j |P_j|} \right)^{1/n} \frac{\sum_{i=0}^{N-1} \omega_{ij}^{\alpha} (z_i - v_j)(z_i - v_j)^T}{\sum_{i=0}^{N-1} \omega_{ij}^{\alpha}} \right\}^{-1}. \tag{12}$$

Let $k = k + 1$ and recycle to (i) until a specified convergence criterion, Δ, is satisfied.

Then $\forall i \in \{0, 1, \ldots, N-1\}$, z_i can be classified to jth class, namely

$$z_i \in \left\{ \Gamma_j | j = \underset{l}{\operatorname{argmax}}(\omega_{il}) \right\}, \tag{13}$$

where Γ_j denotes jth class sample set.

A flow chart of the algorithm is shown in Fig. 3.

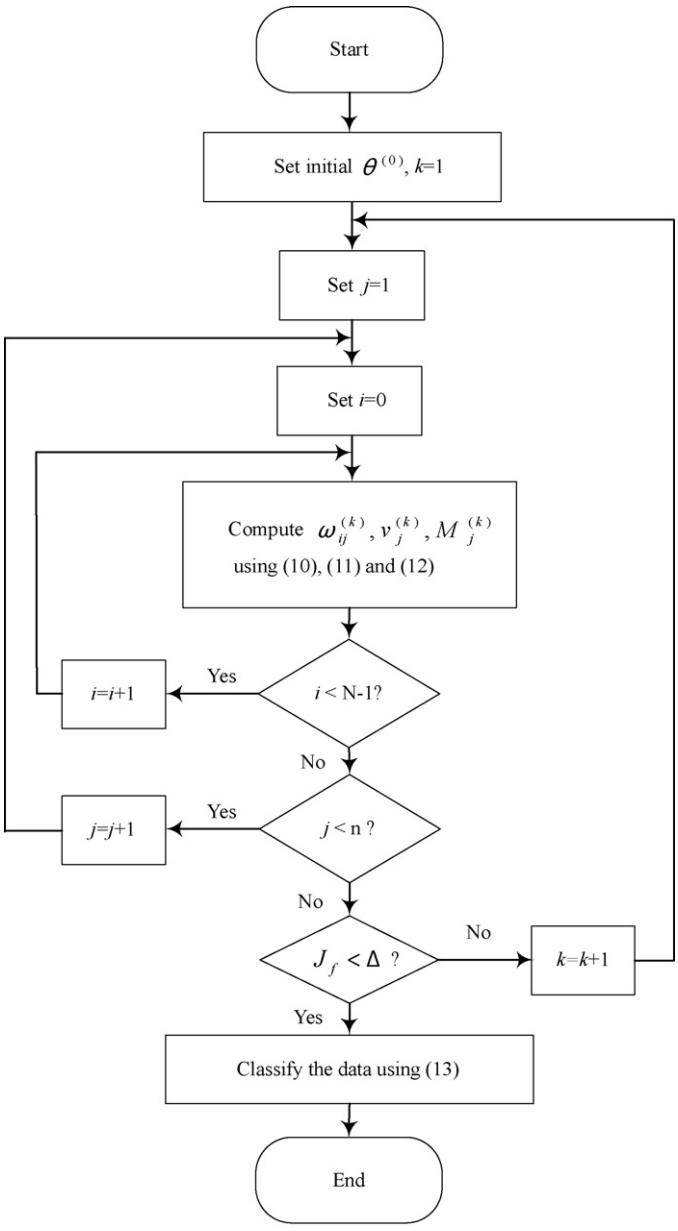

Fig. 3. Flow chart of fuzzy clustering algorithm.

3.2. Identification

The order of the system is determined through the theoretical model. For each data set, we use the following linear model to describe the relationship between the input and output:

$$y_i(k) = \Theta_i^T X_i(k) \quad \forall i \in \{1, 2, \ldots, n\}, \tag{14}$$

where subscript i denotes the ith model, $\Theta_i \in \boldsymbol{R}^{(n_a+n_b+1)\times 7}$ is a system parameter matrix and

$$X_i(k) = (y_i^T(k-1), \ \ldots, \ y_i^T(k-n_a), u^T(k), \ \ldots, \ u^T(k-n_b))^T. \tag{15}$$

Θ_i is unknown and is estimated by the recursive least squares algorithm as

$$\hat{\Theta}_i(k) = \hat{\Theta}_i(k-1) + \frac{a_i X_i(k) e_i^T(k)}{1 + X_i^T(k) X_i(k)}, \tag{16}$$

$$a_i = \begin{cases} 1 & \text{if } \left\| e_i(k) \right\| > M \\ 0 & \text{otherwise} \end{cases}, \tag{17}$$

where $\hat{\Theta}_i$ denotes estimation of Θ_i, M represents the maximum error that can be accepted, and $e_i(k)$ is the output error between the ith model and the practical system, i.e.

$$e_i(k) = y(k) - \hat{\Theta}_i^T X_i(k). \tag{18}$$

The identification results are then expressed as discrete state space equation, i.e.

$$x(k+1) = A_i x(k) + B_i u(k) + B_{di} P_d(k), \tag{19}$$

$$y(k) = C_i^T x(k) + D_i u(k), \tag{20}$$

where $x \in \boldsymbol{R}^{7n_a}$ and P_d denote state variables and power demand, respectively. $A_i \in \boldsymbol{R}^{7n_a \times 7n_a}$, $B_i \in \boldsymbol{R}^{7n_a \times 3}$, $B_{dl} \in \boldsymbol{R}^{7n_a}$, $C_i \in \boldsymbol{R}^{7n_a \times 7}$, $D_i \in \mathbf{R}^{7\times 3}$ are parameter matrices determined by $\hat{\Theta}_i$.

4. Controller design

4.1. Model predictive controller design

Fundamentally, a MPC should predict the output trajectory of a process and compute a series of control actions, subject to constraints, that will minimize the difference between the predicted trajectory and some desired trajectory. A key advantage of the MPC over other control schemes is its ability to deal with constraints in a systematic and straightforward manner.

Generally, the MPC control process consists of future states or output prediction, scrolling optimization, and control signal implementation. Now we use the identified models to design MPC. An important step is to set an objective function, which is defined as

$$\min_{u(k),\ldots,u(k+N_u-1)} J = \sum_{j=1}^{N_u} \Big((\hat{y}(k+j) - y_r(k+j))^T Q (\hat{y}(k+j) - y_r(k+j)) + u^T(k+j) R u^T(k+j) \Big), \tag{21}$$

where N_u is predictive horizon, $\hat{y}(k+j)$ is the estimated output of the system at instant $k+j$ through models based on information available at instant k. $y_r(k+j)$ is the desired output at instant $k+j$, and $Q \in \mathbf{R}^{7\times 7}$, $R \in \mathbf{R}^{3\times 3}$ are weighting matrices on output errors and control, respectively. We choose the control horizon to be equal to the prediction horizon, and define $Q = diag\begin{pmatrix} Q_{\lambda_{O_2}} & Q_{W_{cp}} & Q_{p_{sm}} & Q_{V_{st}} & Q_{I_{st}} & Q_{I_c} & Q_{SOC} \end{pmatrix}$ and $R = diag\begin{pmatrix} R_{V_{cm}} & R_{d_d} & R_{dc} \end{pmatrix}$, where $Q_{\lambda_{O_2}}$, $Q_{W_{cp}}$, $Q_{p_{sm}}$, $Q_{V_{st}}$, $Q_{I_{st}}$, Q_{I_c}, and Q_{SOC} are penalties on errors in λ_{O_2}, W_{cp}, p_{sm}, V_{st}, I_{st}, I_c, and SOC, respectively. $R_{V_{cm}}$, R_{d_d}, and R_{d_c} are penalties on V_{cm}, d_{d} and d_{d}, respectively. We set $Q_{W_{cp}} = 0$, $Q_{p_{sm}} = 0$, $Q_{V_{st}} = 0$, $Q_{I_{st}} = 0$ and $Q_{I_c} = 0$ so that the corresponding outputs are not penalized in the performance index and are only used for checking the constraints.

Remark. The penalty on error in SOC, Q_{SOC}, is set to zero when power demand changes rapidly. In the case of increasing of power demand, it is acceptable that the value of SOC is less than its expected value so that the ultracapacitor can supply more for power peaks. However, if $Q_{SOC} \neq 0$, according to the objective function, SOC will converge to its desired value and then the ultracapacitor will supply less. Similarly, in the case of decreasing of power demand, if $Q_{SOC} \neq 0$, less energy will be charged into the ultracapacitor. When power demand is stable, Q_{SOC} is set to a non-zero value so as to adjust the value of SOC to its desired value. SOC is always also constrained by its lower and upper limits.

Substituting state Eqs. (19) and (20) in (21), the equation is abbreviated as

$$\min_U J = \tfrac{1}{2} U^T \Omega U + (y^T(k) L + G) U, \tag{22}$$

where $\Omega \in \boldsymbol{R}^{3N_u \times 3N_u}$, $L \in \boldsymbol{R}^{7\times 3N_u}$, $G \in \boldsymbol{R}^{1\times 3N_u}$ are constant matrices calculated through the system model and weighting matrices Q, R.

$$U = (u^T(k), u^T(k+1), \quad \ldots, \quad u^T(k+N_u-1))^T. \tag{23}$$

4.1.1. Constraints

One of the most important advantages of MPC is its ability to deal with constraints. In the hybrid fuel cell/ultracapacitor system, several constraints must be observed.

Rapid variation on current will harm the fuel cell, so it is desirable to constrain the rate of change of fuel cell current, i.e.

$$-\Delta I_{max} \leq I_{st}(k+1) - I_{st}(k) \leq \Delta I_{max}, \tag{24}$$

where ΔI_{max} is the upper limit of the rate of change, which is determined by characteristics of the fuel cell.

The ultracapacitor must not be overcharged or overdischarged. The state of charge of the ultracapacitor is an important performance index of the hybrid system, and it should be limited to some desired range

$$SOC_{min} \leq SOC \leq SOC_{max}, \tag{25}$$

where SOC_{min} and SOC_{max} are the lower and upper limits of SOC, respectively. In this paper the SOC is limited between 0.45 and 0.95, and the desired value is 0.70.

Similarly, the ultracapacitor current should not exceed its limitations as

$$-I_{c,max} \leq I_c \leq I_{c,max}, \tag{26}$$

where $I_{c,max}$ is the upper limit of I_c.

Starving the fuel cell of oxygen causes serious life-limiting problems, while supplying it with too much oxygen decreases system efficiency. As a result, the oxygen excess ratio should be limited as

$$\lambda_{min} \leq \lambda_{O_2} \leq \lambda_{max}, \tag{27}$$

where λ_{min} and λ_{max} are the lower and upper limits of oxygen excess ratio, respectively. The value of λ_{O_2} depends on oxygen concentration in the cathode and current drawn from the fuel cell. Generally, the best value of oxygen excess ratio is 2. In this paper the range of λ_{O_2} is constrained between 1.9 and 2.1.

The voltage of the fuel cell, also the bus voltage, is constrained as

$$V_{st,min} \leq V_{st} \leq V_{st,max}, \tag{28}$$

where $V_{st,min}$ and $V_{st,max}$ are the lower and upper limits of V_{st}, respectively.

The duty ratio of the DC/DC converter must, by definition, satisfy the following inequalities:

$$0 \leq d_d \leq 1. \tag{29}$$

$$0 \leq d_c \leq 1. \tag{30}$$

The voltage applied to the compressor motor, V_{cm}, cannot be larger than the rated voltage

$$0 \leq V_{cm} \leq V_{cm,R} \tag{31}$$

Deduced from Eqs. (19)–(21) and inequalities (24)–(31), the control optimization is transformed to the following constrained quadratic programming problem

$$\begin{aligned} &\min_U J = \tfrac{1}{2} U^T \Omega U + (y^T(k) L + G) U \\ &\text{subject to } U_{min} \leq EU \leq U_{max} \end{aligned} \tag{32}$$

where U_{min}, $U_{max} \in \mathbf{R}^8$, and $E \in \boldsymbol{R}^{8\times 3N_u}$ are constant matrices obtained from Eqs. (19) and (20) and inequalities (24)–(31).

4.1.2. Optimization

The constrained quadratic programming problem is then transferred to the following simple optimization problem [17]

$$K\bar{U} + q = F(K\bar{U} + q - \bar{U}), \tag{33}$$

where $\bar{U} \in \boldsymbol{R}^8$ is a variable to be optimized and $q = -E\Omega^{-1}(y^{\mathrm{T}}(k)L + G)^{\mathrm{T}}$, $K = E\Omega^{-1}E^{\mathrm{T}}$, F is a piecewise function of

$$F(\bar{U}) = (F(\bar{U}_1) \cdots F(\bar{U}_8)), \tag{34}$$

and for $i = 1, \ldots, 8$

$$F(\bar{U}_i) = \begin{cases} \bar{U}_{i,min}, & \bar{U}_i < \bar{U}_{i,min} \\ \bar{U}_i, & \bar{U}_{i,min} \le \bar{U}_i \le \bar{U}_{i,max} \\ \bar{U}_{i,max}, & \bar{U}_{i,max} < \bar{U}_i \end{cases} \quad (35)$$

where $\bar{U}_{i,\min}$ and $\bar{U}_{i,\max}$ are the minimum and maximum values of $\bar{U}_i$, respectively.

If $\bar{U}^*$ is a solution of Eq. (33), then the optimal solution of the quadratic programming problem (32) is

$$U^* = \Psi \bar{U}^* + \vartheta, \quad (36)$$

where $\Psi = \Omega^{-1}E^T$, $\vartheta = -\Omega^{-1}(y^T(k)L + G)^T$.

$\bar{U}$ can be optimized through the structure shown in Fig. 4.

MPCs are designed for each linear model, but only one will operate online during each period. This optimization method can also be implemented through neural network and it has a faster convergence rate than related optimization methods.

4.2. Adaptive switch design

We describe next the adaptive switch that defines which MPC operates online during each control period. We define a performance criterion function of the ith model as

$$J_{s,i} = \gamma e_i^2(k) + \mu \sum_{j=k-l+1}^{k} e^{-\tau(k-j)} e_i^2(j), \quad i = 1, \ \ldots, \ n, \quad (37)$$

where γ, μ, τ are constants and l is an integer. $e_i(k)$ denotes the error between output of the ith model and output of the practical system, i.e.

$$e_i(k) = \hat{y}_i(k) - y(k). \quad (38)$$

The adaptive switch controller periodically compares the performance criterion function and switches on the MPC designed for the jth model.

$$j = \underset{i}{\operatorname{argmin}} \sum_{i=1}^{n} J_{s,i}. \quad (39)$$

The design procedure and operating principle of the proposed modeling and control method can be summarized as the following:

(I) Classify the real-world data according to the flow chart in Fig. 3.
(II) Identify parameters $\hat{\Theta}_i$ using Eq. (16) and establish state space models (19) and (20).
(III) Choose a model based on (39).
(IV) Optimize $\bar{U}$ according to Fig. 4.
(V) Compute control variable U^* using (36).
(VI) Control the system.
(VII) If there is no power demand, classify the new collected data and update models of the system, else go to (III) and start next control period.

Table 1
Parameters used in the experiment and simulation.

Sym.	Meaning	Value
T_{st}	Temperature of fuel cell	338 K
T_{atm}	Atmospheric temperature	288 K
P_{H_2}	Partial pressure of hydrogen	1.5 atm
n	Number of cells in each stack	260
A	Active area of fuel cell	140 cm^2
C	Capacitance of ultracapacitor	86 F
$V_{c,max}$	Maximum voltage of ultracapacitor	168 V

5. Experiment and simulation

The hybrid system, as shown in Fig. 1, is designed to power a car. The rated power is 50 kW. The DC bus voltage is controlled between 170 V and 250 V. The PEM fuel cell is composed of two PEM fuel cell stacks, which are connected in parallel. Each stack has 260 cells and an active area of 140 cm^2.

The ultracapacitor is 86 F and the maximum voltage is 168 V. The value of capacitance can be realized by a bank of 56 standard ultracapacitors, each with capacitance of 4800 F and a rated voltage of 3 V, connected in series. The maximum stored energy is 304 Wh ($1/2 \times 86 \times 168^2/3600 \times 0.95^2$), although only 97 Wh ($1/2 \times 86 \times 168^2/3600 \times (0.70^2 - 0.45^2)$) is available between the target nominal *SOC* and the lower limit. This 97 Wh corresponds to an average power at 35 kW for 10 s and that is sufficient to buffer the fuel cell from acceleration transients.

The experiments and simulations described in this section relied on Matlab/Simulink and were developed in two steps. First, models of the hybrid system were developed from real-world data from the system. Second, multiple models-based MPCs were designed to control the hybrid fuel cell system and comparisons between constrained and unconstrained MPCs were made.

5.1. Modeling experiment and simulation

Real-world input and output data of a 50-kW PEM fuel cell was collected. Assuming hydrogen pressure, humidity, and temperature of the stacks are constant. Related parameters used are shown in Table 1.

The sampled data are equally divided into two groups. One group is used for modeling and the other is used for validating. In modeling phase, we first classify the real-world data into 5 sets using fuzzy clustering, and then we identify 5 models according to each data set based on Eqs. (16)–(18). In each control period, the most suitable model is chosen from the 5 models through Eq. (39) to calculate the output of the system. Simulation result of PEM fuel cell modeling is shown in Fig. 5. It is shown that there always exists a model that adequately represents the practical system and the multiple models closely match the practical fuel cell. Multiple linear models of other components of the hybrid system, such as DC/DC converter and ultracapacitor are established based on their mechanistic models.

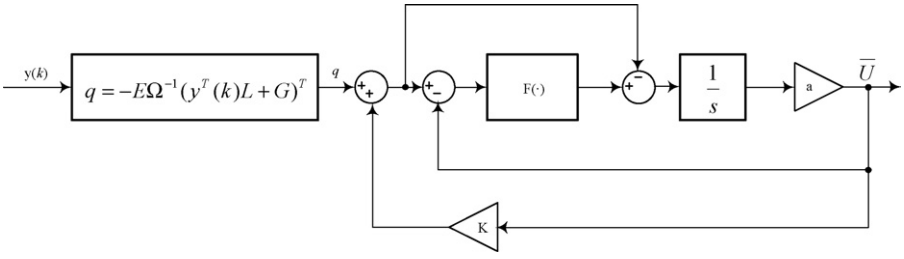

Fig. 4. Diagram for optimization. $F(\cdot)$ is the piecewise function (34), $a > 0$ is a scaling constant.

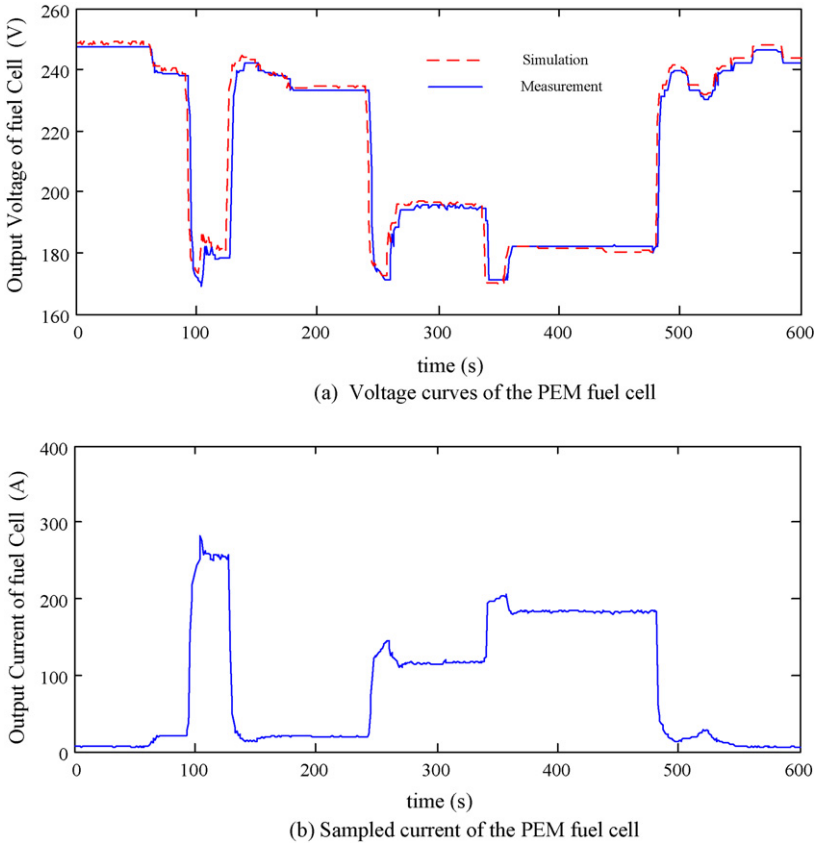

Fig. 5. Simulation of using the multiple models. 5 models are used in the modeling. (a) Voltage curves of the PEM fuel cell and (b) sampled current of the PEM fuel cell.

5.2. Control simulation

Control performances of constrained and unconstrained MPCs are studied and compared to validate the proposed constrained MPC. The design of unconstrained and constrained MPCs is similar and is described as the follows.

Based on multiple models established previously, MPCs for each model and the adaptive switch are designed and implemented in Matlab/Simulink. The output weighting matrix Q is empirically set as $Q = diag(100, 0, 0, 0, 0, 0, 10)$, where 100 is the penalty for λ_{O_2} and 10 is the penalty for *SOC*. It is noted here that the penalty for λ_{O_2} is much higher than that of *SOC*. This is because, in the hybrid system, oxygen excess ratio is the most important index and should be controlled with high priority. The penalty for *SOC* is set to zero in case of rapid change of power demand.

The input weighting matrix, R, which includes penalties for air compressor voltage and duty ratio of the DC/DC converter, is set as $R = diag(0.001, 100, 100)$. Since the compressor voltage is usually over 100 V and duty ratio is no more than 1, the two penalties for duty ratios (100) are much larger than that of compressor voltage (0.001). In addition, control horizon is set to 10 sampling steps. The constraints of the constrained MPC are listed in Table 2.

Table 2
Constraints for the constrained MPC.

Sym.	Meaning	Lower limit	Upper limit
ΔI_{max}	Rate of change of fuel cell current	$-20\,A\,s^{-1}$	$20\,A\,s^{-1}$
SOC	State of charge of the ultracapacitor	0.45	0.95
I_c	Current of the ultracapacitor	−250 A	250 A
λ_{O_2}	Oxygen excess ratio	1.9	2.1
V_{st}	Voltage of the fuel cell	170 V	250 V
V_{cm}	Voltage of the air compressor	0	200 V

A typical urban driving cycle in China is used in simulation and the power profile, as shown in Fig. 6, is considered as the power demand.

The simulation results for both the unconstrained and the constrained MPC are shown in Fig. 7.

It is noticed that, in Fig. 7(a), there exist significant perturbations in oxygen excess ratio that fluctuates between 1.58 and 2.28 for unconstrained MPC. As a result, oxygen starvation is unavoidable in this situation. While in the case of the constrained MPC, the oxygen excess ratio is relatively stable and only varies between 1.92 and 2.07, which is a much narrower range than for the unconstrained MPC. This is because of the constraints on oxygen excess ratio and the rate of change of fuel cell current.

As shown in Fig. 7(b) and (c), current and voltage are much smoother when using the constrained MPC than when using the unconstrained MPC. The maximum rate of change of the fuel cell is $20\,A\,s^{-1}$, which is the upper limit of the rate. The voltage curve is inside the limited area and stable. These phenomena prove that the constraint on voltage and current change rate is valid. If capacitance of the ultracapacitor increases, the upper limit of the current change rate can be set lower. As a result, there is a tradeoff between upper limit of the change rate of fuel cell current and capacitance of the ultracapacitor.

In Fig. 7 (d), the variation of *SOC* of the ultracapacitor is much larger when using the constrained MPC than when using the unconstrained MPC. This is because, under the constrained MPC, much more energy is squeezed out from the ultracapacitor to supply the peak load demands, and so smooth perturbations of fuel cell current. The *SOC* satisfies the constraints on lower and upper limits. Therefore, the constraints on *SOC* are effective. In case of rapid

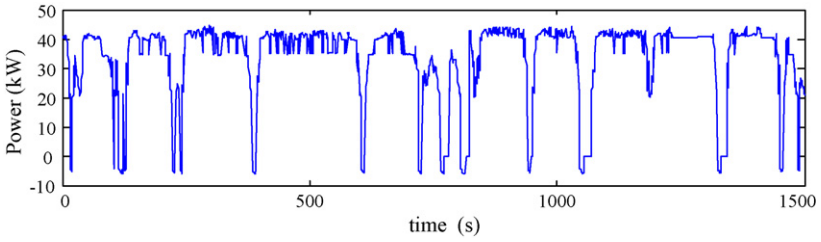

Fig. 6. Power demand imposed by the driving cycle.

change of power demand, penalty on *SOC* in weighting matrix *Q* is set to zero. In this situation *SOC* is only constrained by its lower and upper limits, and the ultracapacitor discharges more or charges more energy to smooth the fuel cell transient. As a result, a good tradeoff between the transient of the fuel cell and ultracapacitor can be achieved, according to constraints and weighting matrices of the output errors.

The power distribution under the constrained MPC is shown in Fig. 8. It is seen that the fuel cell power is smooth while the frequent high power demands are distributed to the ultracapacitor. The change rate of the fuel cell current and power are low. Moreover, main variables (e.g., λ_{O_2}, *SOC*, I_c) meet their constraints. Consequently, the hybrid system is well protected, which is helpful to extend the lifetime of the system.

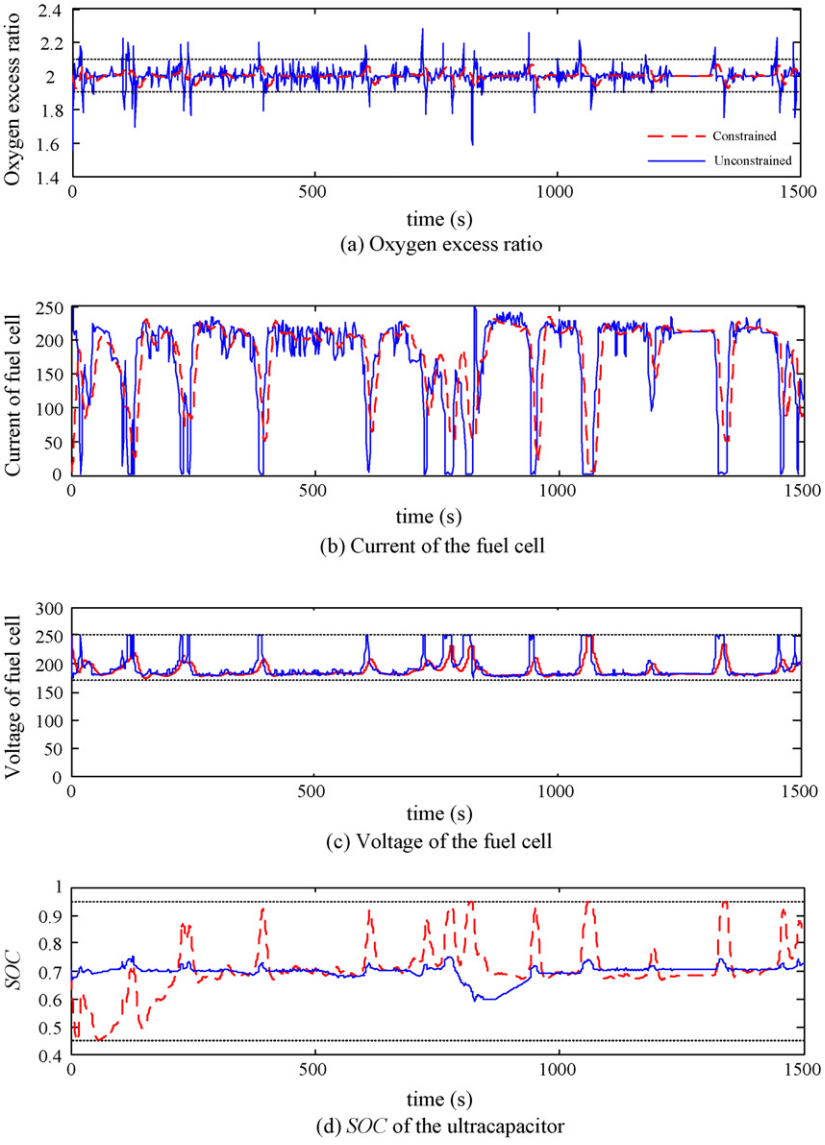

Fig. 7. Simulation results of constrained (red line) and unconstrained (blue line) MPC. The weighting matrices are $Q = diag(100, 0, 0, 0, 0, 0, 10)$, $R = diag(0.001, 100, 100)$. (a) Oxygen excess ratio; (b) current of the fuel cell; (c) voltage of the fuel cell and (d) *SOC* of the ultracapacitor. (For interpretation of the references to colour in this figure legend, the reader is referred to the web version of the article.)

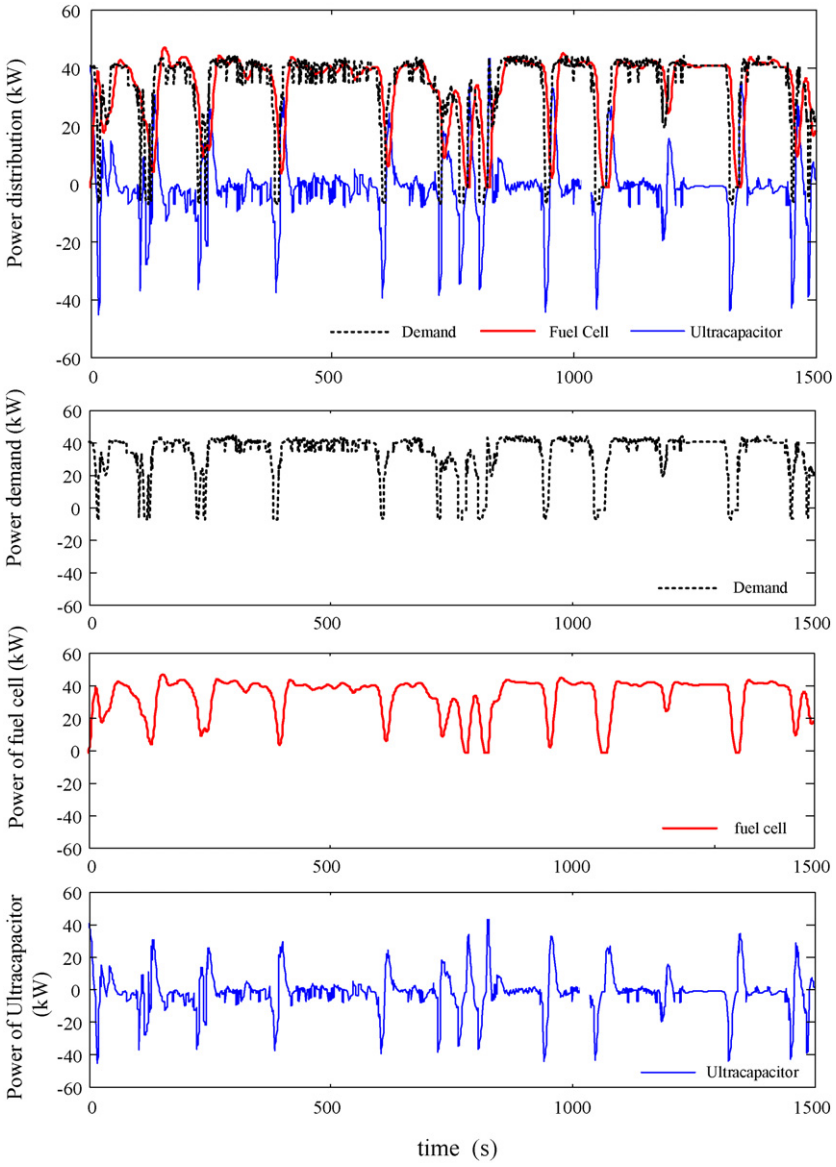

Fig. 8. Power distribution of the hybrid system.

6. Conclusion

A centralized multiple models-based constrained MPC for a hybrid fuel cell/ultracapacitor system was proposed and verified. The proposed approach, different from other approaches described in the literature, can provide a globally optimized solution for power distribution and oxygen control, and can protect the hybrid system from oxygen starvation by trading off transient current demand from the PEM fuel cell to the ultracapacitor. It achieves this by setting constraints and by weighting output errors.

Acknowledgements

This work was supported by the National Science Foundation of China under contract 60705032, and received partial support from the US Office of Naval Research under contract N00014-07-1-0611. The authors wish to thank the reviewers for constructive comments based on which this paper has been improved.

References

[1] A. Vahidi, A.G. Stefanopoulou, H. Peng, IEEE Transactions on Control Systems Technology 14 (6) (2006) 1047–1057.
[2] T. Zhu, S.R. Shaw, S.B. Leeb, IEEE Transactions on Energy Conversion 21 (1) (2006) 195–201.
[3] Z.H. Jiang, L.J. Gao, R.A. Dougal, IEEE Transactions on Energy Conversion 22 (2) (2007) 507–515.
[4] A.A. Ferreira, J.A. Pomilio, G. Spiazzi, L.D.A. Silva, IEEE Transactions Power Electronics 23 (1) (2008) 107–115.
[5] Y. Guezennec, T.-Y. Choi, G. Paganelli, G. Rizzoni, Proceedings of the American Control Conference (2003) 2055–2061.
[6] P. Rodatz, G. Paganelli, A. Sciarretta, L. Guzzella, Control Engineering Practice 13 (2005) 41–53.
[7] X. Zhang, C.C. Mi, A. Masrur, D. Daniszewski, Journal of Power Sources 185 (2008) 1533–1543.
[8] J.T. Pukrushpan, H. Peng, A.G. Stefanopoulou, Journal of Dynamic Systems, Measurement, and Control 126 (1) (2004) 14–25.
[9] J.T. Pukrushpan, A.G. Stefanopoulou, H. Peng, Control of Fuel Cell Power Systems: Principles, Modeling, Analysis and Feedback Design, Springer-Verlag, London, UK, 2004.
[10] A. Vahidi, A.G. Stefanopoulou, H. Peng, Proceedings of the American Control Conference 1 (2004) 834–839.
[11] J. Sun, I. Kolmanovsky, IEEE Transactions on Control Systems Technology 13 (6) (2005) 911–920.

[12] P.-F. Tsaia, J.-Z. Chub, S.-S. Jang, Journal of Process Control 13 (2002) 423–435.
[13] L.-X. Wang, F. Wan, Automatica 37 (2001) 1235–1243.
[14] Y. Fu, T.Y. Chai, Automatica 43 (2007) 1101–1110.
[15] S. Filler, M. Perrin, A. Jossen, Journal of Power Sources 96 (2001) 113–120.
[16] D.E. Gustafson, W.C. Kessel, Proceeding of the IEEE Conference on Decision and Control 17 (1) (1978) 761–766.
[17] Y.S. Xia, G. Feng, J. Wang, Neural Networks 17 (2004) 1003–1015.